Modeling of Shrinkage Behavior in Cement Paste Using Thermal-structural Interaction

Tzu-Chau Chen[*1], Peter G. Ifju[2]
[1,2]University of Florida
*Corresponding Author: 2370 SW Archer Rd Gainesville, FL 32608, jimchen@ufl.edu

Abstract: This paper describes using thermal-structural interaction to model the shrinkage behavior in cement paste under drying. An inverse method of combining the finite element analysis and the least-squares method is implemented to fit experimentally determined shrinkage in order to obtain material properties from the complex geometry used in the tests. The finite element model is created based on thermal-structural interaction with the transient analysis. In this multi-physics model, moisture diffusion in the specimen is modeled as heat transfer. And shrinkage behavior is modeled as thermal expansion. Once the material properties are obtained, the shrinkage behaviors of cement paste in different drying, or geometric conditions, and in the ring test are simulated. Their results were compared with those from the moiré interferometry experiments to validate the constructed model.

Keywords: shrinkage, moisture diffusion, cement paste, moiré interferometry

1. Introduction

One of the fundamental characteristics of concrete materials is shrinkage. Shrinkage can influence the development of tensile stress and cause subsequent cracking in concrete structures when external or internal constraints exist. To better assess the structural life of concrete materials, investigation of the shrinkage behavior is extremely important. Also, shrinkage in concrete materials is not uniform over the entire specimen but highly dependent upon the distribution of moisture content. As known, moisture distribution is mainly governed by moisture diffusion during drying, which is here described by Fick's law and self-desiccation in the hydration process [1, 2]. Also, moisture distribution is generally described with relative humidity instead of moisture concentration. From the previous research, shrinkage from self-desiccation or shrinkage in sealed conditions is negligible for w/c ratio=0.5. In this case, the measured shrinkage can be assumed as drying shrinkage only. Therefore, only drying effect or moisture diffusion is considered in the model if w/c=0.5 was used. In other words, if w/c is below 0.4, shrinkage from self-desiccation must be considered.

The inverse approach [3-5] to obtain the material properties of shrinkage from the complex geometry used in the tests is shown. Two materials parameters, the film coefficient and the shrinkage coefficient, are defined and to be determined. Optimization in conjunction with the finite element model was used to fit experimentally obtained shrinkage in order to determine these two material parameters. The finite element model as the forward model is created based on thermal-mechanical interaction. In this coupled model, moisture diffusion is modeled as heat transfer problem and shrinkage behavior is modeled as thermal expansion in mechanical model. Table 1 shows the details of using the analogy regarding to the models. Once they are obtained, they can be the inputs for finite element analysis to predict the shrinkage under different drying or geometric conditions. The moiré interferometry tests can be performed and their results can be compared with FEA to validate the constructed model and the obtained material properties.

Moiré interferometry is an optical technique to measure the full-field in-plane displacements and strains with high sensitivity [6]. The outputs are a set of the fringe patterns representing the intensity distribution from the interference between two rays of laser. Traditionally, the fringe patterns are analyzed manually by locating the positions and counting the fringe numbers based on intensity which is a point-wise method. Although this method can be repeated on multiple data points, it is time intensive and errors in the results are inevitable because of the uncertainty in determining the exact location of a fringe. The methods based on extraction of the underlying phase distribution are becoming popular since they have significant advantages over the intensity-based methods: data is

obtained on a full field basis, not just at the fringe maxima and minima, the sign of the deformation is given and immunity from noise is normally better [7]. Here, an automated strain analysis system based on phase shifting theory is used to obtain the full-field information on the cement paste specimens.

2. Numerical Model

2.1 Finite Element Model

The finite element model takes advantage of axisymmetry because the geometry of the specimen in the tests is a cylindrical disk. Axisymmetric model can save running time while using the inverse approach to determine the material properties. The expression of moisture diffusion coefficient as thermal conductivity used in this study is shown as below

$$D = D_1 * (\alpha + \frac{1-\alpha}{1+(\frac{1-h}{1-h_c})^n})$$

where D_1 is the maximum of $D(h)$ for h =1.0, $\alpha=D_0/D_1$, D_0 is the minimum of $D(h)$ for h = 0.0, h_c is the pore relative humidity when $D(h)$ = $0.5D_1$. Here D_1 =25, α=0.05, n=6, and h_c =0.72 as recommended in the literature for room temperature [8]. Typical values E=2.5GPa and ν=0.3 are used for cementitious materials in the model. The shrinkage coefficient and the film coefficient are two unknown material properties to be determined by the inverse approach.

2.2 Initial Condition

Before the specimen is maintained in the chamber, it is assumed that h=1 or 100% when t=0 which refers to Day 1 in the experiment results.

2.3 Boundary Condition

The boundary conditions for moisture diffusion model are described in figure 1. The insulation on the boundary along the symmetrical line is automatically assumed. The grating on top of the specimen cannot be assumed as the insulation to moisture flux. The value of the diffusion coefficient D_g of the epoxy, which is very water resistant, is $2x10^{-7}$ mm^2/s ($0.01728mm^2/day$). When the grating is very thin compared with thickness of the concrete specimen, the boundary condition at the interface between the grating and the specimen can be described by the equation (1) [9]. The flux on the other two boundaries is assumed as convection type which is described by the equation (2). Here, f represents the film coefficient. J represents moisture flux. h_s represent relative humidity on the surface. h_{en} represents ambient relative humidity. t_g represents the thickness of the grating, which is 0.1 mm here. No boundary conditions need to be defined in the mechanical model because the specimen in the experiments is in the condition of free shrinkage.

$$J = D_c * grad(h) = D_g \frac{(h_s - h_{en})}{t_g} \quad (1)$$

$$J = D_c * grad(h) = f * (h_s - h_{en}) \quad (2)$$

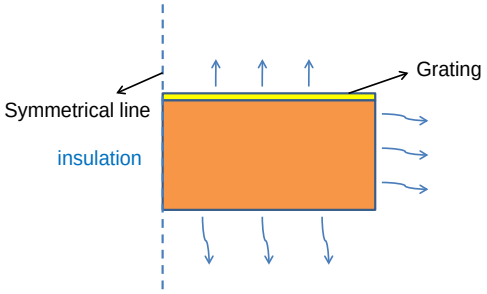

Figure 1. Boundary conditions in moisture diffusion model

2.4 Inverse Method

In the inverse method, the finite element model described above is the forward model created in COMSOL. This forward model is interfaced with the optimization code which is developed in Matlab to obtain the shrinkage coefficient and the film coefficient. The shrinkage coefficient and the film coefficient are two variables in the optimization code. In each of iterations, the optimization code specifies the values of these two variables, calls the forward model to solve the problem, and then computes the value of the objective function. When the value of the objective function is minimized, which indicates the fitting of the FEA result with

the experimental data is optimized, the shrinkage coefficient and the film coefficient are hence determined. The optimization code is based upon the nonlinear least-squares method and the Gauss-Newton algorithm is adopted. The objective function is defined as the following equation:

$$F(\varepsilon, f) = \sum_{j=1}^{m}\sum_{i=1}^{n}(E_{ij} - e_{ij})^2 \qquad (3)$$

In the above formulation, there are two unknown coefficients represented by constant ε as the shrinkage coefficient and f as the film coefficient. E_{ij} in equation (3) is the ith radial strain on jth drying day obtained experimentally and e_{ij} is the radial at the same point computed using finite element analysis. It is assumed that there are n such experimentally obtained radial strains at n positions from the center to the circumference on the surface with the grating. Here, n is equal to 6 and the measurement positions are equally spaced. Hence, the distance between two neighboring positions is 2.8mm. And m represents the total drying duration in the chamber in units of day. Here, m is equal to 6, which corresponds to drying duration of 6 days in the experiments.

Using the experimentally obtained radial strains under RH=50% and room temperature at six locations from Day 2 to Day 7, the estimation of these two material parameters is performed through the inverse approach mentioned above. The curve fitting result is shown in figure 2. The shrinkage coefficient ε=53.30 με / ºC and the film coefficient f= 2.02 mm/day are obtained.

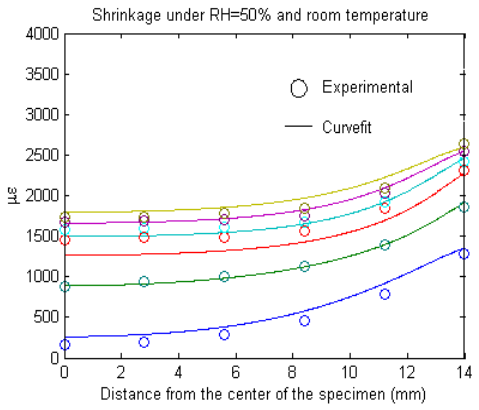

Figure 2. Optimization results.

Once the shrinkage coefficient and the film coefficient are determined, they can be the inputs for 3-D finite element model to predict concrete shrinkage behavior in different conditions. By selecting the surface of interest, FEA results can be compared with the experimental results from moiré in 2D x-y coordinate. Moreover, 3D model can demonstrate the true shrinkage behavior inside of the concrete. This relates the experimental data to the concrete behavior inside a structure.

3. Validation of Model

In order to validate the constructed model and the obtained material properties, the tests in different surrounding humidity, in different geometric condition, and the ring test are performed and their results are compared with those simulated by FEA.

3.1 Different Surrounding Humidity

The same material properties are used to predict the shrinkage under room temperature and RH=80% which is created with saturated sodium chloride solution. The size of the specimen remains the same. The experimental and FEA results from Day 2 to Day 7 are shown as figure 3. Only the Day 3 full-field experimental and FEA strain maps are shown as figure 4. The experimental data do not match with FEA result exactly for every day. However, the trend and the range of magnitude of shrinkage are very similar.

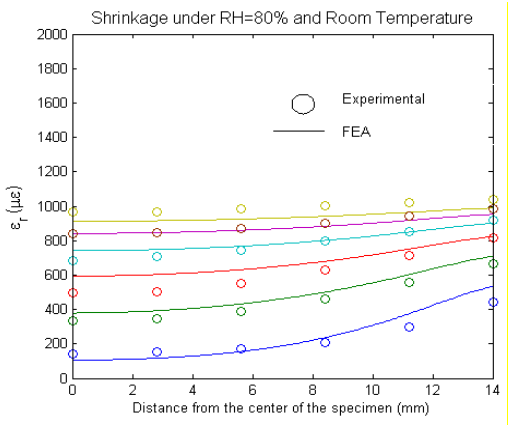

Figure 3. Experimental and FEA results for RH=80% and room temperature.

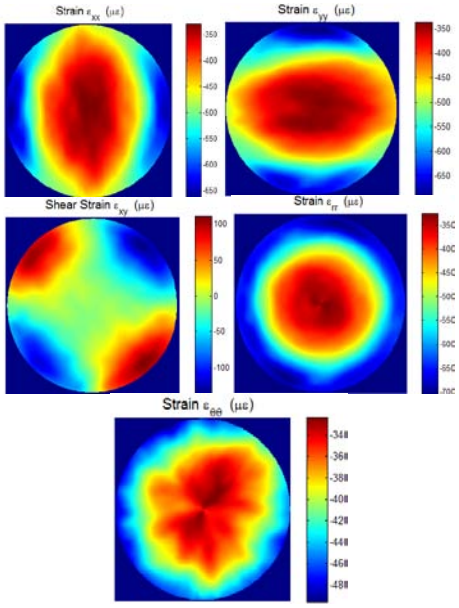

(a)

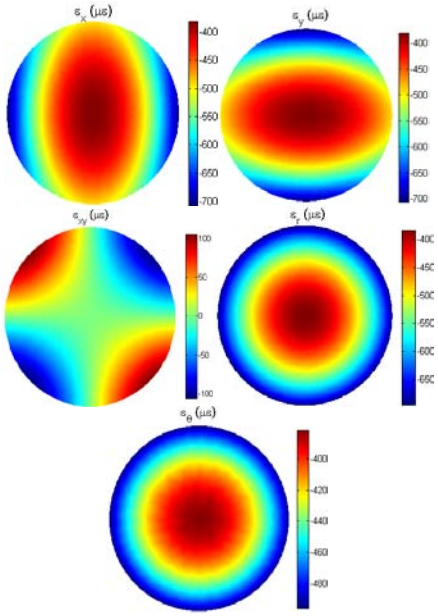

(b)

Figure 4. Experimental (a) and FEA (b) results for RH=80% and room temperature on Day 3.

3.2 Different Geometry Condition

The square-shape cement paste specimen with w/c=0.5 is made with the size of 25 mm in length and 14 mm in thickness. The same process is used to prepare grating on the surface the specimen. The specimen is stored in the chamber of 80% RH and room temperature for three day3 after demold. The U and V-field moiré fringe patterns from Day 1 to Day 4 are recorded. The distribution of $\mathcal{E}_{xx}$ from the center of the specimen to the outer surface is shown in figure 5. The full-field experimental and FEA maps for Day 4 are shown as figure 6. However, the displacement and normal strain in y direction are not shown here due to symmetry.

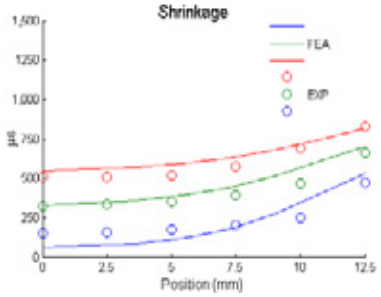

Figure 5. Distribution of $\mathcal{E}_{xx}$ from the center of the specimen to the outer surface.

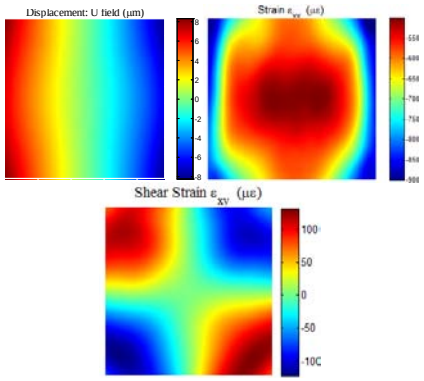

(a)

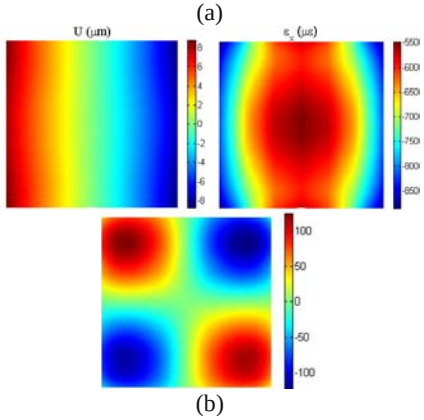

(b)

Figure 6. Experimental (a) and FEA (b) maps for square specimen on Day 4.

From figure 6, the experimental result does not match well with FEA result for every day measurements. However, they are similar in the range of the magnitude and the trend. Figure 6 shows that the maximum in-plane normal strain occurred in the four corners of the specimen. The maximum shear strain does not occur exactly in the corners but near the corners. Also, FEA and the experimental results have good agreement in the displacement field.

3.3 Ring Test

In the ring test, the thin epoxy layer is formed on the silicone rubber grating as the procedure of replication of grating. The steel rod of 14 mm in diameter and 11 mm in thickness is placed in the middle of the mold and then cement paste fluid is poured around the steel rod. The positions of the mold and the steel rod are marked on the back side of the master grating in advanced. After demolded, the specimen is stored in room temperature and RH60% which is stable in the laboratory. The U and V-field moiré fringe patterns from Day 1 to Day 3 are recorded. A 3-D composite model is created in the finite element analysis with the typical values E=200 GPa and ν=0.33 for the steel rod in the test.

The Day 2 and Day 3 moiré fringe patterns are analyzed through the automatic fringe analysis system and the full-field strain maps in x-y coordinate are shown as figure 7 for Day 2 and figure 8 for Day 3. FEA results are also included in the figures for the purpose of comparisons. However, the full-field strain maps do not show information concerning the steel rod not only because it is not the focus in the research but also because its deformation is insignificant compared with the portion of the cement paste by observing the fringe patterns. The maximum normal and shear strains move toward the steel rod instead of remaining near the outer surface.

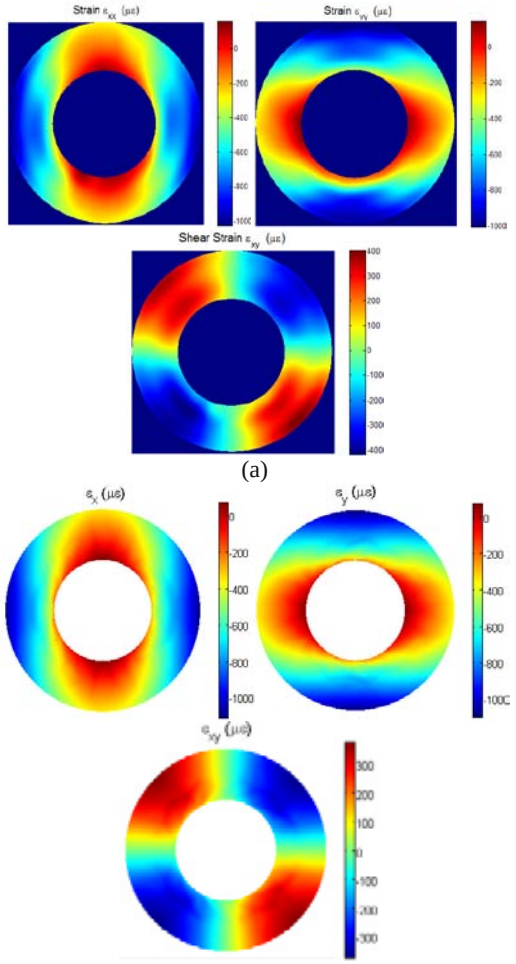

Figure 7. Experimental (a) and FEA (b) strain maps for the ring test on Day 2.

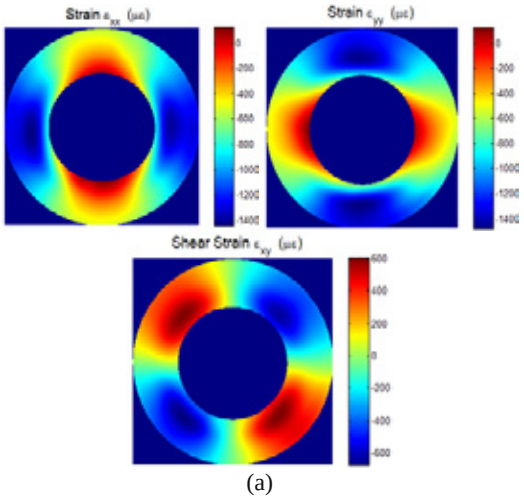

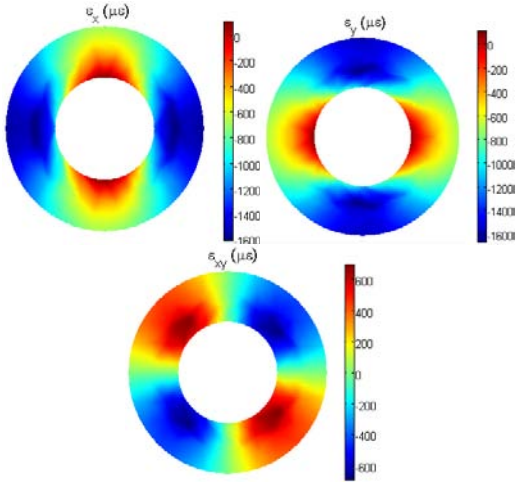

(b)

Figure 8. Experimental (a) and FEA (b) strain maps for the ring test on Day 3.

4. Conclusions

The moiré interferometry technique is used to measure the shrinkage in cement paste. An automated strain analysis system is developed to obtain the full-field displacement and strain maps. A numerical method of combining the finite element model and the nonlinear least-squares method is developed to obtain the material properties from the complex geometry used in the tests. The tests in different drying condition, or in different geometry condition, and the ring test are performed and their results have good agreement with FEA results.

5. References

1. Sakata, K., 'A study on moisture diffusion in drying and drying shrinkage of concrete', Cement and Concrete Research 13 (2) 216-224, (1983)
2. T. Ayano, F.H. Wittmann, "Drying, moisture distribution, and shrinkage of cement-based materials," Materials and Structures, Vol.35, 134-1140 (2002)
3. Padmanabhan S., Huner J.P., Kumar A.V., Ifju P.G., "Load and Boundary Condition Calibration using Full-field Strain Measurement," Experimental Mechanics, Vol.46, p569–578 (2006)
4. Wang Z., Cardenas-Garcia J.F., Han B., "Inverse Method to Determine Elastic Constants Using a Circular Disc and Moiré´ Interferometry," Experimental Mechanics, Vol.45, No.1, p27-34 (2005)
5. Fu G., Moosa A.G., "An optical approach to structural displacement measurement and its application." Journal of Engineering Mechanics, Vol.128, No.5, p511-520 (2002)
6. Post, D., Han, B., Ifju, P.G., High Sensitivity Moiré: Experimental Analysis for Mechanics and Materials, Spring-Verlag, New York (1994)
7. Bazant, Z. P., Najjar, L.J., 'Nonlinear water diffusion in nonsaturated concrete', Mater.
8. Huntley, J. M., "Automated fringe pattern analysis in experimental mechanics: a review," Journal of Strain Analysis, Vol.33, No 2, p105-125 (1998)
9. Jang C., Han B., "Analytical Solutions of Gas Transport Problems in Inorganic/Organic Hybrid Structures for Gas Barrier Applications," Journal of Applied Physics, Vol.105, 093532 (2009)

6. Acknowledgements

The authors are grateful to Florida Department of Transportation (FDOT) for the financial support.

7. Appendix

Table 1: The analogy of thermal-mechanical model

<table>
<tr><td colspan="2">Thermal Mechanical Interaction Model</td></tr>
<tr><td>Thermal Model</td><td>Mechanical Model</td></tr>
<tr><td>Heat Transfer
vs.
Moisture Diffusion</td><td>Thermal Expansion
vs.
Shrinkage</td></tr>
<tr><td>Temperature
vs.
Relative Humidity</td><td rowspan="3">Thermal
Expansion coefficient

vs.

Shrinkage coefficient</td></tr>
<tr><td>Conductivity
vs.
Diffusity</td></tr>
<tr><td>Surface coefficient
vs.
Film coefficient</td></tr>
</table>